Biointerface Research in Applied Chemistry
Platinum Open Access Journal (ISSN: 2069-5837)

Article
Volume 11, Issue 3, 2021, 10572 - 10584
https://doi.org/10.33263/BRIAC113.1057210584

Chitosan-Modified Silver Nanoparticles Enhance Cisplatin Activity in Breast Cancer Cells

Sayuri Gounden [1], Aliscia Daniels [1], Moganavelli Singh [1,*]

[1] Nano-Gene and Drug Delivery Laboratory, Discipline of Biochemistry, University of KwaZulu-Natal, Private Bag X54001, Durban, South Africa
* Correspondence: singhm1@ukzn.ac.za;

Scopus Author ID 37095919000

Received: 15.09.2020; Revised: 25.10.2020; Accepted: 27.10.2020; Published: 1.11.2020

Abstract: Cancer therapy has been hindered by treatments lacking sensitivity, specificity, and affordability. The side effects of conventional chemotherapy enforce the need for a treatment strategy that would maximize the anti-cancer activity of the drug while minimizing its' adverse effects on healthy cells. Nanoparticles (NPs) as carriers for anti-cancer drugs have attracted interest due to their favorable properties, which include the enhanced permeability and retention effect. Silver NPs (AgNPs) have been explored as nanocarriers owing to their good conductivity, chemical stability, and therapeutic potential. In this study, AgNPs were synthesized, functionalized with chitosan (CS), and loaded with the anti-cancer drug cisplatin (CIS). Successful conjugation, size distribution, and morphology of the NPs were assessed by UV-vis and Fourier transform infra-red (FTIR) spectroscopy, NP tracking analysis (NTA), and transmission electron microscopy (TEM). The encapsulated CIS (>80%) was efficiently and rapidly released from the nanocomplex at low pH, favoring delivery to a tumor micro-environment. Cytotoxicity profiles of the CS-AgNP-CIS nanocomplexes exhibited significant cell death in the human breast cancer cell lines, MCF-7 and SKBR-3. They were more effective than the free drug, exhibiting >50% cell death. Our results demonstrate a potentially efficient anti-cancer drug delivery system with selectivity to breast cancer cells.

Keywords: Silver nanoparticles; cisplatin; chitosan; breast cancer; nanocomplexes; drug delivery.

© 2020 by the authors. This article is an open-access article distributed under the terms and conditions of the Creative Commons Attribution (CC BY) license (https://creativecommons.org/licenses/by/4.0/).

1. Introduction

Cancer is a growing concern for society, with recent studies predicting a 75% increase in the number of cancer cases globally, with a formidable 78% increase expected in developing countries by the year 2030 [1]. Breast cancer is a life-threatening disease and a leading cause of female mortality worldwide [2]. Conventional chemotherapeutic drugs, such as cisplatin (CIS), have been clinically proven to combat different types of cancers including sarcomas, and cancers of soft tissues, bones, muscles, and blood vessels [3]. CIS, a potent high molecular weight platinum-based compound, induces cell cycle arrest and apoptosis in most cancer cell types by forming intra- and inter-strand adducts with DNA [4]. Its mode of action is predominantly due to its ability to crosslink with the purine bases on DNA, interfering with DNA repair mechanisms, and successively inducing apoptosis in cancer cells [3,5].

Unfortunately, most anti-cancer drugs lack sensitivity and specificity, leading to unpleasant side effects in patients due to high therapeutic doses. Hence, there is a need for novel treatment strategies to mitigate these problems. The application of nanoparticles (NPs) has favorably impacted the medical field leading to many researchers turning to nanomedicine

for the treatment of diseases, including cancer [5]. Apart from reducing the adverse effects of the drug, NPs have been observed to offer protection of the drug from degradation as well as in improving the bioavailability of the drug [6, 7]. Among the NPs being investigated, silver has shown good conductivity, chemical stability, outstanding therapeutic potential apart from their antibacterial properties [8,9]. Silver nanoparticles (AgNPs) have been explored as delivery vehicles of therapeutic material to diseased cells. AgNPs, however, have shown the tendency to aggregate and progress into larger clusters that deviate from the nanoscale and diminishes the efficiency of a nano delivery system, and opposing its application [10]. Hence, natural polysaccharides, which are environmentally benign, biodegradable, highly abundant, and affordable, are regarded as favorable stabilizers for synthesized AgNPs. The deacetylated product of chitin, chitosan, has exhibited intriguing biological activities such as biocompatibility, biodegradability, non-toxicity, non-antigenicity, and adsorption, ideal for drug delivery [6, 11, 12]. It was reported that functionalization with a 0.5% (w/v) concentration of CS effectively stabilized the synthesized AgNPs, to enable their use in biomedical applications, such as drug delivery [11,13,14]. It has been observed that the addition of targeting ligands to nano complexes aid in the active targeting of cancer cells. However, certain nano-drug delivery systems display selectivity towards specific types of cancer cells, negating the use of targeting moieties, as large-scale production of targeted delivery systems introduces a high-cost factor to the pharmaceutical industry, as well as challenges in design and characterization [15, 16]. As evidenced in the literature, limited studies have been conducted on the evaluation of CIS conjugated AgNPs functionalized with a CS biopolymer. This study evaluates the sensitivity and specificity of CS functionalized AgNPs as delivery vehicles of CIS to the human cancer cells, Caco-2 (colorectal adenocarcinoma), MCF-7 (breast adenocarcinoma), HepG2 (hepatocellular carcinoma) and SKBR-3 (breast adenocarcinoma), and the non-cancer HEK293 (embryonic kidney) cells.

2. Materials and Methods

2.1. Materials.

Silver nitrate ($AgNO_3$), tri-sodium citrate ($Na_3C_6H_5O_7.2H_2O$), phosphate-buffered saline tablets [PBS, (140 mM NaCl, 10 mM phosphate buffer, 3 mM KCl)], 3-[(4,5-dimethylthiazol-2-yl)-2,5-diphenyl tetrazolium bromide] (MTT), ethidium bromide, glacial acetic acid, dimethyl sulfoxide [DMSO] and cisplatin (Mw: 300 $g.mol^{-1}$, $Pt(NH_3)_2Cl_2$) were supplied by Merck (Darmstadt, Germany). Chitosan ≥ 75% deacetylated (Mw: 1000-5000), 10% polysorbate 20 (Tween 20), triphenyl phosphate (TPP), acridine orange hemi (zinc chloride) salt [3,6-Bis(dimethylamino) acridine hydrochloride zinc chloride double salt], and dialysis tubing (MWCO= 1000 Daltons) were supplied by Sigma-Aldrich Chemical Co., (St. Louis, MO, USA). The human cells, embryonic kidney (HEK293), colorectal adenocarcinoma (Caco-2), hepatocellular carcinoma (HepG2), and breast adenocarcinoma (MCF-7 and SKBR-3) were obtained from the American type culture collection, Manassas, Virginia, USA. Sterile fetal bovine serum (FBS) was supplied by Hyclone GE Healthcare (Utah, USA). Eagle's Minimum Essential Medium (EMEM) with L-glutamine, Penicillin/ Streptomycin/ Amphotericin B (100x) antibiotic mixture, and trypsin-versene-EDTA mixture were supplied by Lonza Bio-Whittaker (Verviers, Belgium). All sterile tissue culture plasticware were sourced from Corning Inc. (New York, USA). All reagents used were of analytical grade, and ultrapure (18 MOhm) water (Milli-Q Academic, Millipore, France) was used throughout**.**

2.2. Synthesis of AgNPs, CS-AgNPs, and CS-AgNP-CIS.

AgNPs were synthesized by the reduction of silver nitrate ($AgNO_3$) with tri-sodium citrate ($Na_3C_6H_5O_7$), adapted from previous publications [17-19]. Briefly, 50 ml of $AgNO_3$ (0.001 M) in ultrapure H_2O was heated with stirring to 95°C. Thereafter, 5 ml of tri-sodium citrate (1% w/v) was added dropwise to the $AgNO_3$ solution. After continuous stirring for 10 min, a color change from clear to a deep yellow indicated the successful formation of AgNPs [18, 20]. The solution was stored in the dark at room temperature due to the light sensitivity of the synthesized AgNPs [10]. The final theoretical concentration of the AgNP solution was 1.58 mM (0.17 mg/ml), and was utilized for functionalization with CS and conjugation of CIS.

2.2.1. Formation of CS-AgNPs.

Approximately, 1.25 ml of Tween 20 (0.5% v/v) was added to 2.5 ml of CS (0.5 mg/ml in 1% acetic acid) with constant stirring [16]. TPP (1.25 ml, 2 mM), was then added to CS solution in a 2:1 (CS:TPP, v/v) ratio, with stirring for 3 hours. Thereafter, 5 ml of AgNPs was added dropwise to the CS solution in a 2:1 ratio of AgNP:CS (v/v), and stirred overnight [6]. The AgNPs were then pelleted by centrifugation at 2000 rpm for 15 min, resuspended in 18 MOhm water [9], and stored at 4°C.

2.2.2. Formulation of CS-AgNP-CIS.

Briefly, 2.5 ml of CIS (0,47 mg/ml, 1.58 mM) was added to 2.5 ml of TPP activated CS (2.2) under constant stirring for 3 hours to ensure adequate absorption of CIS to CS. Thereafter, 7.5 ml of the AgNP (2.1) solution was added dropwise to the CS:CIS solution to obtain a 2:1:1 ratio of AgNP:CS:CIS [6, 22]. This solution was stirred over 24 hours, and the CS-AgNP-CIS pelleted by centrifugation as previously.

2.3. Characterization of nanoparticles and nanocomplexes.

2.3.1. UV-vis Spectroscopy.

UV-vis spectroscopy (Jasco V-730 Bio Spectrophotometer, Tokyo, Japan) was used to determine the absorbance spectra of the AgNPs, CS-AgNP, and CS-AgNP-CIS nanocomplex, using water as a control. The successful synthesis of the AgNPs was confirmed by a surface plasmon absorbance at 400 nm, with shifts in the peak indicating successful functionalization with CS or conjugation of CIS [18].

2.3.2. Fourier Transform Infra-Red Spectroscopy (FTIR).

FTIR was utilized to verify the presence of essential bonds and functional groups in the synthesized NPs. The samples were analyzed using a Spectrum Perkin Elmer Spectrophotometer, with the respective IR spectra from 4000 cm^{-1}-380 cm^{-1}, obtained using Spectrum Analysis Software.

2.3.3. Nanoparticle Tracking Analysis (NTA).

NTA is a visualization technique that determines the hydrodynamic size, concentration, and zeta potential measurements [23], and was conducted using a Nanosight NS-500 (Malvern

Instruments, Worcestershire, UK) operating at 25 °C. Samples (1 ml) were analyzed in triplicate to ensure the validity of the results obtained.

2.3.4. Transmission Electron Microscopy (TEM).

TEM was conducted to determine the ultrastructural morphology of all NPs and nanocomplexes. Approximately 10 µl of each sample was positioned on a 400 mesh carbon-coated copper grid (Ted Pella Inc. Redding, USA)**,** air-dried at room temperature, and viewed using a JEOL-JEM T1010 electron microscope (Jeol, Tokyo, Japan) at 60 000x magnification and 100 kV acceleration voltage. The visualized TEM images were captured and analyzed using the iTEM Soft Imaging Systems (SIS) Megaview III fitted with a side-mounted 3-megapixel digital camera.

2.4. Drug encapsulation efficiency.

The CS-AgNP-CIS sample was sonicated for 15 min, and vortexed before determining absorbance at 300 nm, to obtain the total CIS present in the sample [3]. The sample was then centrifuged at 2000 rpm for 15 min to separate the CS-AgNP-CIS nanocomplex from the free unbound drug. The supernatant was removed, and absorbance of the unbound drug measured (Jasco V-730 Bio Spectrophotometer, Tokyo, Japan), at 300 nm**.** The encapsulation efficiency (EE) of the nanocomplex CS-AgNP-CIS was determined using equation 1 [6].

$$EE\ (\%) = (\text{Total CIS}) - (\text{Unbound CIS}) / (\text{Total CIS}) \times 100 \quad (1)$$

2.5. Drug release studies.

The amount of drug liberated from the CS-AgNP-CIS nanocomplex was determined over a 72-hour period at pH 4.5, 5.0, 6.5, and 7.4. This served to investigate the pH-responsive behavior of the nanocomplex [21]. Approximately 1 ml of the nanocomplex was added to four separate dialysis tubes (1000 MWCO), and suspended in beakers filled with 5 ml of PBS at the respective pHs. Absorbance readings of the PBS (30 µl) were taken at 4-hour intervals for 72 hours, at a wavelength of 300 nm. An equivalent amount of PBS was replaced to maintain the sink volume. A drug release profile was generated at each pH using the amount of drug encapsulated within the nanocomplex, as reference.

2.6. In vitro cytotoxicity.

Cells (HEK293, Caco-2, MCF-7, SKBR-3, HepG2), were seeded into 96-well plates (containing 100 µl EMEM, 10% (v/v) FBS and 1% antibiotics), at a seeding density of 2.5 x 10^4 and incubated for 24 h at 37°C in 5% CO_2. The medium in the wells was thereafter replenished, and the NPs and nanocomplexes were introduced in triplicate at 5, 10, 15, 25, and 50 µg. Free CIS was included at the theoretical amounts within the nanocomplex to ensure an accurate comparative study. The cells were incubated over a period of 48 hours at 37°C, after which the medium was replenished with fresh growth medium (100 µl) containing 10 µl of a 5 mg/ml (in PBS) MTT stock and incubated for 4 hours at 37°C [24, 25]. This medium/MTT was then removed, and the resultant formazan crystals were solubilized in 100 µl of DMSO. The optical densities (OD) were determined at 540 nm using a Mindray MR-96A microplate reader (Vacutec, Hamburg, Germany), with DMSO as the blank. Cell viabilities (%) were calculated using equation 2.

$$\text{Cell Viability} = (OD_{treated} / OD_{control}) \times 100\% \quad (2)$$

2.7. Apoptosis Assay.

The assessment of apoptosis was performed by staining the cells with the vital dual dye system of acridine orange and ethidium bromide [26, 27]. Cells at a density of 1.5 x 10^5 cells/well were seeded into a 48-well plate (250 µl medium per well) and incubated at 37 °C for 24 hours. Thereafter, the medium was replenished, and the cells were treated with the respective NPs and nanocomplexes, corresponding to their IC_{50} values, and incubated for 48 hours at 37 °C. The assay was conducted in triplicate with untreated cells used as positive controls. Following incubation, the cells were washed with 200 µl PBS, followed by staining with 10 µl of the acridine orange(AO) /ethidium bromide (EB) dye solution (100 µg/ml AO and 100 µg/ml EtBr in PBS) with shaking for 5 min. The dye was removed by washing the cells with PBS (200 µl), and cells viewed under an Olympus fluorescent microscope (200x magnification). Images were captured using a CC12 fluorescence camera (Olympus Co., Tokyo, Japan).

2.8. Statistical analysis.

All data has been presented as a mean ± standard deviation (± SD, n=3). The Dunnetts' post hoc test was used for the MTT assay. The statistical significance of the tests was set at **p<0.01 and *p<0.05. Each of the experimental values was compared to their corresponding control. The software used for statistical analysis was Microsoft Excel™ 2016.

3. Results and Discussion

3.1. UV-vis and FTIR spectroscopy.

UV-vis spectroscopy is sensitive to the presence of Ag colloids, as the surface plasmon resonance (SPR) of these NPs display an intense absorption peak in the 350 - 450 nm region. The plasmon absorption displays a redshift as the NP size increases upon the addition of the different moieties. The successful formation of AgNPs was exhibited by a peak at a wavelength of 418 nm (Figure 1) correlating to previous reports [10,18]. This single peak indicated no by-products after AgNP synthesis [18]. Successful functionalization with CS was seen as a shift in the SPR from a wavelength of 418 nm to 422 nm for the CS-AgNP functionalized nanoparticle. A shift in the peak from a wavelength of 422 nm to 472 nm for the CS-AgNP-CIS nanocomplex indicated successful conjugation of CIS to CS-AgNP.

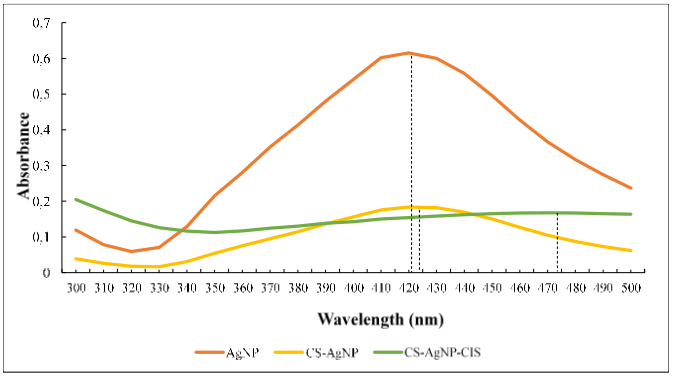

Figure 1. UV-vis spectroscopy of AgNP; CS-AgNP and CS-AgNP-CIS.

From the FTIR spectra (Figure 2), CS displayed a characteristic IR peak at 3126 cm^{-1} correspondings to the N-H, O-H stretch; the NH^{3+} peak for the CS-AgNP is present at approximately 1667 cm^{-1}, with the C-O stretching seen at approximately 1010 cm^{-1}. For the CS-AgNP-CIS nanocomplex the characteristic amide peak of CS shifted from 1667 m^{-1} to 1718 cm^{-1}, indicating conjugation of CIS to CS. Peak assignments were done according to the literature [7, 28].

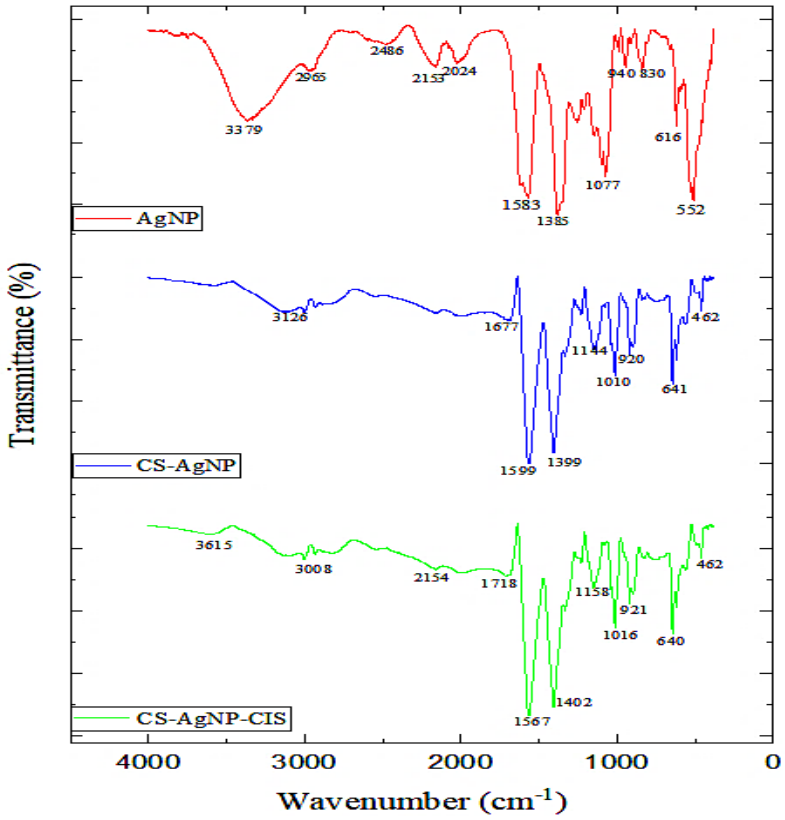

Figure 2. FTIR spectra of AgNP; CS-AgNP and CS-AgNP-CIS.

3.2. NTA and TEM.

NTA directly visualizes and sizes NPs in aqueous solutions, offering exceptional insight into the true size distributions of the NPs in solution, which is at the heart of determining the benefits of targeted drug delivery [23]. From Table 1, it can be seen that the size of the NPs increased upon incorporation CS and CIS, confirming successful conjugation. The hydrodynamic sizes obtained were below 122 nm, with possible aggregation and swelling of the NPs in a solution being accounted for. This high-resolution hydrodynamic particle size distribution is beneficial since the size of the nanocomplex can influence cellular uptake, the release of the bound drug, as well as the immune responses [10]. It has been observed that the overall particle size may exceed 200 nm upon drug binding, which will reduce its potential in drug delivery [29]. Prior to functionalization, the zeta potential of the AgNP was -35.1 ± 0.4 mV, indicating electrostatic stabilization of AgNPs due to the ionization of the polar citrate carboxyl groups present on the surface, correlating to previous studies [9]. The zeta potential of the CS-AgNPs increased to 10.3 mV, confirming observations that CS with its high amino content aids in positively charging NPs for drug delivery [14]. After conjugation of CIS, the zeta potential increased to 33.2 mV, promoting ideal properties for treatment with CS-AgNP-CIS, as this intensely positive nanocomplex would readily attract the negatively charged cell

surface. The high zeta potential value further suggests good colloidal stability for enhanced delivery of the drug [30].

Table 1. The sizes and zeta potentials of the nanoparticles and nanocomplex as obtained from NTA.

NP/Nanocomplex	Size Distribution	Zeta Potential
AgNP	53.9 ± 0.2 nm	-35.1 ± 0.4 mV
CS-AgNP	109.9 ± 34.1 nm	10.3 ± 0.1 mV
CS-AgNP-CIS	121.7 ± 19.3 nm	33.2 ± 0.0 mV

TEM (Figure 3) revealed smooth spherical NPs and nanocomplexes, displaying uniformity in both shape and size, and within the nanosized range of 22-30 nm in diameter. Aggregation of AgNPs prior to functionalization was evident (Figure 3A), and is similar to other reports for AgNPs at these concentrations [31]. CS-AgNPs (Figure 3B) displayed monodispersity, indicating that CS aided in preventing the agglomeration of the AgNPs. A layer of CS is indefinably visible around the AgNP. Conjugation of CIS was not only evident by the slight increase in size but also by the color intensity of the nanocomplex, indicating an increase in density.

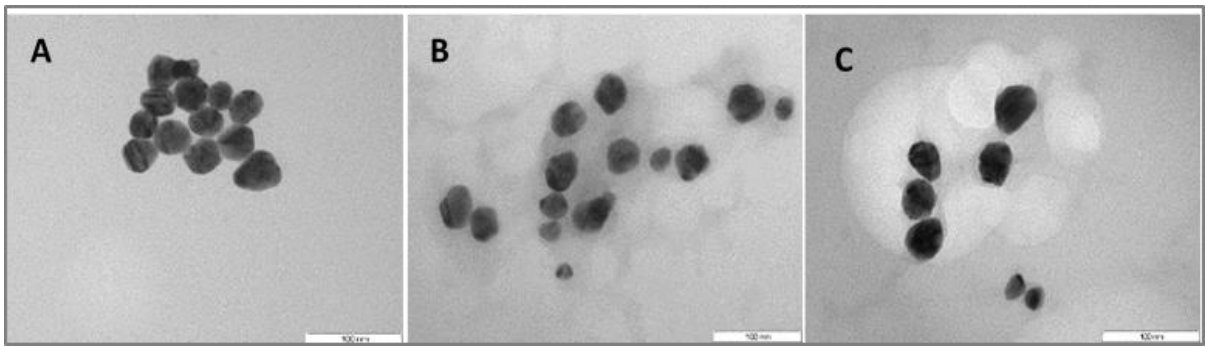

Figure 3. TEM of **A**: AgNP; **B:** CS-AgNP; **C:** CS-AgNP-CIS. Scale bar = 50 nm.

3.3. Encapsulation efficiency.

The CIS encapsulation efficiency in CS-AgNP was assessed using UV-vis spectroscopy. The encapsulation efficiency of CIS in the CS-AgNP-CIS nanocomplex was calculated to be 84.5%. This high encapsulation efficiency is in accord with the corresponding increase in the size of the nanocomplex after the conjugation of the drug. The relatively high encapsulation efficiency may have also been plausibly influenced by the concentration of CS used in the study. An increase in the absorption of a poorly soluble drug at an optimal concentration of 0.5 mg/ml of CS was reported [21, 32].

3.4. Drug release studies.

The drug release profile of CS-AgNP-CIS was generated at pH 4.5, 5.0, 6.5, and 7.4 to determine the pH-responsive behavior of the developed nanocomplex in simulated *in vivo* conditions. Figure 4 illustrates the pH dependency of the nanocomplex, releasing approximately 60% of the encapsulated CIS rapidly after 8 hours at the lowest pH of 4.5 and 98% after 48 hours.

The amount of CIS continuously released from the nanocomplex is inversely proportional to the pH of the PBS used in the study, as a minimal 52% of CIS was released after 48 hours at a pH of 7.4. The pH-dependency of the nanocomplex was possibly induced

by a large number of amino groups present on CS, which solubilize at low pH, releasing the drug [21, 32].

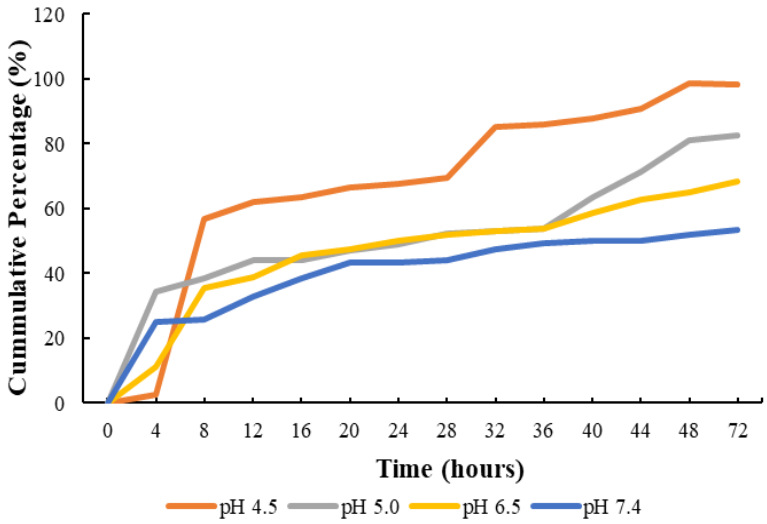

Figure 4. Drug release of CIS from the CS-AgNP-CIS nanocomplex at pH 4.5, pH 5.0, pH 6.5, and pH 7.4.

This is favorable as pH 6 or lower is easily accomplished in tumor tissues due to lactic acid produced as a by-product of anaerobic glucose metabolism. Even lower pH values of 3.0–5.5 are feasible in acidic intracellular organelles, such as endosomes and lysosomes, within cancer cells, leading to more CIS being released in the ideal tumor micro-environment with increased toxicity to the cells. The nanocomplex displayed aptness for treatment as a minimal drug is released at a neutral pH, which is the environment for the growth of healthy cells, thereby decreasing the level of cytotoxicity on normal cells and reducing side effects. However, further studies and mathematical modeling [33,34] may be warranted to produce a model for this drug release mechanism.

3.5. *In vitro* cytotoxicity.

Cell viability is measured when metabolic events leading to cell death either from necrosis by underlying cytotoxic effects or naturally inducing apoptosis [35]. AgNPs and CS-AgNPs showed a similar trend with some dose-dependent cytotoxicity in the HEK293 cells (Figure 5 A). Decreased healthy kidney cell viabilities were observed upon treatment with AgNPs in a dose-dependent manner, correlating to these results [10]. CS-AgNP-CIS did not induce much cell death compared to free CIS at the same concentrations. This could be due to the pH dependency of the CS-AgNP-CIS nanocomplex, releasing a mere 52% of CIS over a 48-hour period in HEK293 cells at pH 7.4. This result bodes well for the use of CS-AgNP-CIS as an anti-cancer delivery system since it produced minimal toxicity in these non-cancer cells compared to the treatment of CIS on its own. In the Caco-2 cells (Figure 5B), AgNPs on their own did produce toxicity below 30% at most concentrations tested and had a similar trend to the CS-AgNP-CIS and CIS alone. This was also evident in the MCF-7 cells (Figure 5C), possibly due to the higher susceptibility of these two cell lines to Ag^{+} ions, as previously reported [36]. The CS-AgNP-CIS nanocomplex exhibited favorable lower cell viabilities than the free CIS in the MCF (Figure 5C) and SKBR-3 cells (Figure 5D). The drug release profile links to the cytotoxicity profile for CS-AgNP-CIS, as the nanocomplex released large quantities of CIS at lower pH corresponding to the micro-environment of cancer cells. Comparatively,

the free CIS performed the best in the Caco-2 (Figure 5B) and HepG2 cells (Figure 5E). This indicated that the nanocomplex had some specificity towards the breast cancer cells [31] while the free CIS was more specific for the colon (Caco-2) and liver (HepG2) cancer cells.

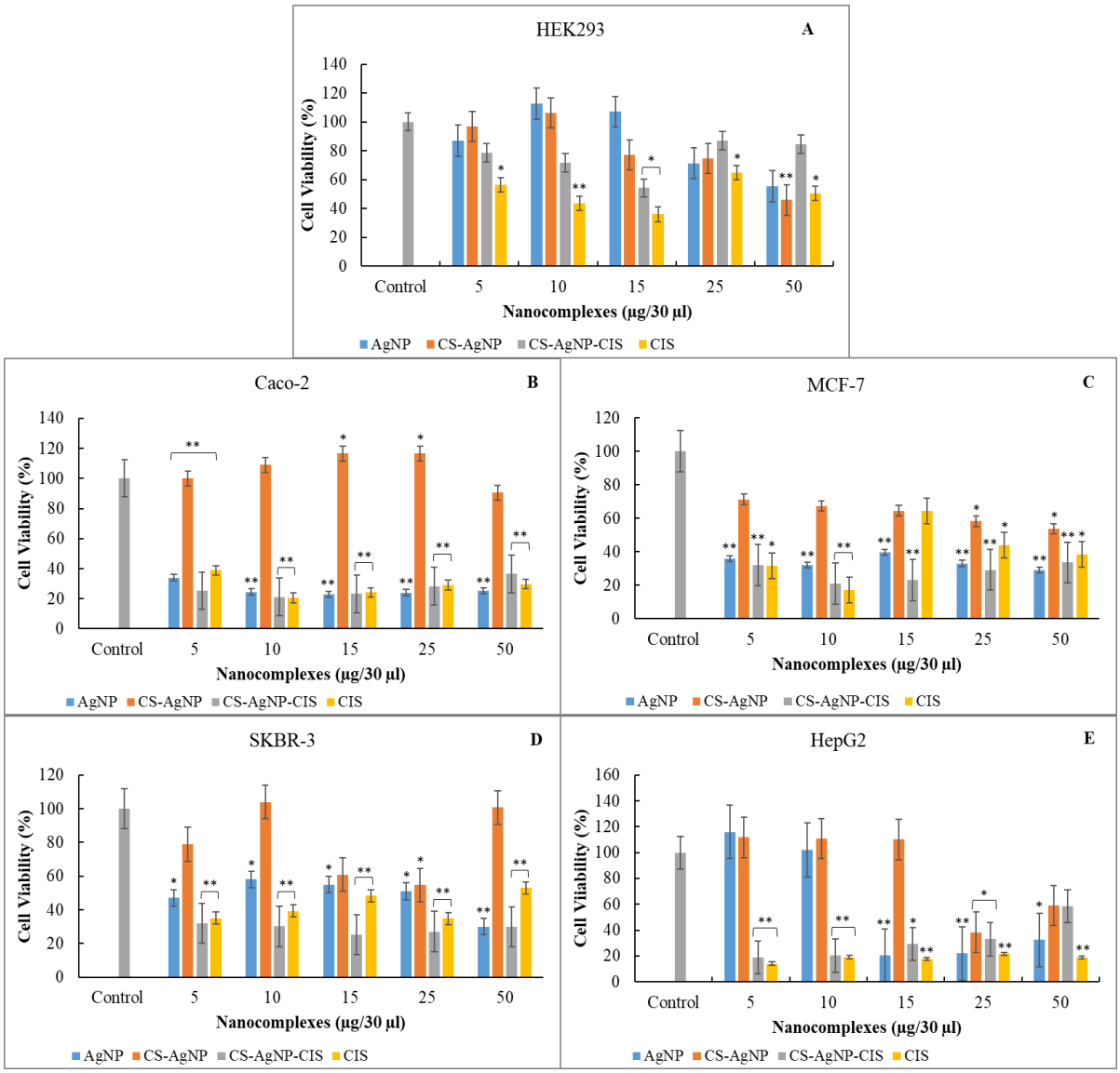

Figure 5. MTT cytotoxicity profile of nanocomplexes against (A) HEK293, (B) Caco-2, (C) MCF-7, (D) SKBR-3, and (E) HepG2 cells. Data are represented as means ± SD (n=3), *p<0.05, **p<0.01 were considered statistically significant.

Overall, the nanocomplex significantly reduced cell viabilities of the cancer cells at the lower doses (25 µg and below). This corresponds to reports that the treatment of AgNPs from 1-10 µg/ml [37] and its nanocomplexes at doses from 25 µg to 300 µg exhibited an increase in cell viability in HeLa cells [31]. This could be due to these nanocomplexes being readily taken up by the tumor cells at lower concentrations. In contrast, at higher concentrations, the nanocomplexes tend to aggregate, increasing in size, and have a challenge traversing the cellular membrane [10]. The HepG2 cells (Figure 5E), however, presented with the lowest cell viabilities for the nanocomplex, similar to that for the free CIS. AgNPs of smaller than 5 nm have been reported to have higher toxicities [38], and those of 10 nm in size showing lower cytotoxicity [39], boding well for these synthesized AgNPs and their nanocomplexes. Overall, this system has provided an indication of anti-cancer specificity for the treatment of breast cancer and can be further optimized and explored.

The IC_{50} calculations were conducted in order to determine the dose of treatment at which 50% of cell death was achieved [40]. The IC_{50} values (Table 2) for the CS-AgNP-CIS nanocomplex and free CIS were compared, and revealed that the breast cancer cell lines not only required lower doses to achieve 50% cell death but that the CS-AgNP-CIS nanocomplex was active at lower quantities than free CIS. The toxicity of CIS at high doses has been reported [41]. This result further confirmed that the drug-loaded nanocomplex had higher anti-cancer activity in the breast cancer cells than CIS on its own.

Table 2. IC_{50} (µg)values for CS-AgNP-CIS and CIS.

CELLS	CS-AgNP-CIS	CIS
HEK293	635	12.69
Caco-2	1227.6	0.0582
MCF-7	1.66	16.16
SKBR-3	5.46	21.97
HepG2	46.35	2.35

3.6. Apoptosis assay.

Apoptosis is known to play a significant role in cellular homeostasis [42]. The principle of this study involved acridine orange (AO) permeating all cells, resulting in nuclei fluorescing green and ethidium bromide (EB) being taken up by cells that have lost cytoplasmic membrane integrity, with the nuclei fluorescing red. Green indicated live cells, red apoptotic cells, and orange necrotic cells [26, 43].

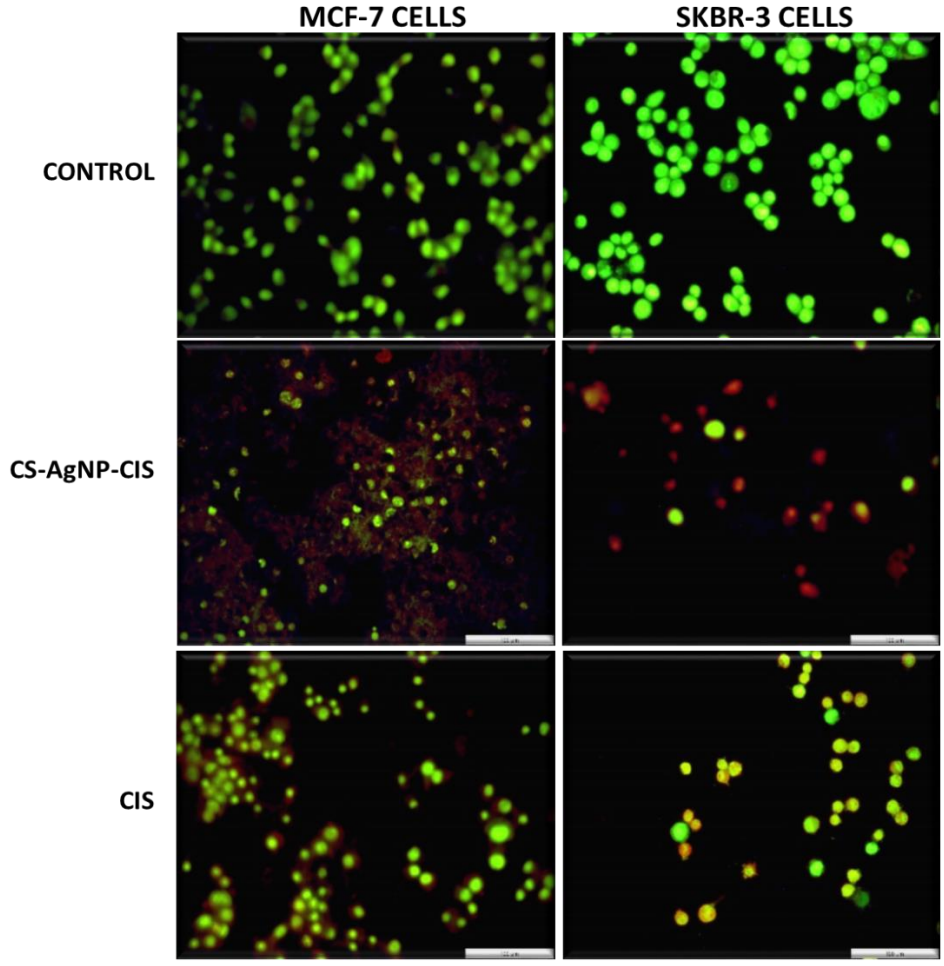

Figure 6. Fluorescent images of acridine orange/ethidium bromide (AO/EB) stained cells showing apoptosis induction by CS-AgNP-CIS and CIS in MCF-7 and SKBR-3 cells.

Hence, cells in various stages of apoptosis can be visualized. Since the breast cancer cells were most affected by the nanocomplexes, their images are represented in Figure 6, and is compared against CIS in inducing apoptosis. The anti-cancer activities noted in this apoptosis assay correlated to the trend of cytotoxicity. The breast cancer cell lines, MCF-7 and SKBR-3, displayed immoderate red fluorescence of apoptotic cells after treatment with the nanocomplex compared to the free drug. Loss of morphology is also evident, similar to reports using AgNPs and other NPs in MCF-7 cells [33,34,39]. This apparent cell specificity could possibly be due to the unique morphology, microenvironment as well as mono-dispersity of the breast cancer cells, which promoted optimum delivery of CIS by the nanocomplexes [2,16].

4. Conclusions

This chitosan functionalized AgNP nano delivery system demonstrated favorable characteristics such as small size, high positive zeta potential, and successfully encapsulated more than 80% cisplatin. Furthermore, this system displayed specificity towards breast cancer cells, with over 80% cell death at doses less than 10 µg, and exhibited minimal cytotoxicity in the non-cancer cells, without the use of a targeting moiety. This is encouraging for future studies and further investigations both *in vitro* and *in vivo* to further our understanding of the mechanism of the cytotoxicity induced by these nanocomplexes. Overall, the results of this study provide basic and crucial information for the development of other such therapeutic delivery systems for the future treatment of diseases such as cancer and based on our results, specifically breast cancer.

Funding

This research was funded by the National Research Foundation of South Africa, grant numbers 113850/ 81289.

Acknowledgments

The authors acknowledge colleagues of the Nano-Gene and Drug Delivery group for continued support.

Conflicts of Interest

The authors declare no conflict of interest. The funders had no role in the design of the study; in the collection, analyses, or interpretation of data; in the writing of the manuscript, or in the decision to publish the results.

References

1. Siegel, R.L.; Miller, K.D.; Jemal, A. Cancer Statistics, 2019. *CA-Cancer J. Clin.* **2019**, *69*, 7–34, https://doi.org/10.3322/caac.21551.
2. Bray, F.; Ferlay, J.; Soerjomataram, I.; Siegal, R.L.; Torre, L.A.; Jemal, A. Global cancer statistics 2018: GLOBOCAN estimates of incidence and mortality worldwide for 36 cancers in 185 countries. *CA-Cancer J. Clin.* **2018,** *68,* 394-424, https://doi.org/10.3322/caac.21492.
3. Florea, A.M.; Büsselberg, D. Cisplatin as an Anti-Tumor Drug: Cellular Mechanisms of Activity, Drug Resistance and Induced Side Effects. *Cancers* **2011**, *3*, 1351–1371, https://doi.org/10.3390/cancers3011351.
4. Ghosh, S. Cisplatin: The first metal based anti-cancer drug. *Bioorg. Chem*. **2019**, *88*, https://doi.org/10.1016/j.bioorg.2019.102925.

5. Maney, V.; Singh, M. The synergism of Platinum-Gold bimetallic nanoconjugates enhance 5-Fluorouracil delivery in vitro. *Pharmaceutics* **2019**, *11*, https://doi.org/10.3390/pharmaceutics11090439.
6. Nivethaa, E.A.K.; Dhanavel, S.; Narayanan, V.; Vasu, C.A.; Stephen, A. An *in Vitro* Cytotoxicity Study of 5-Fluorouracil Encapsulated Chitosan/gold Nanocomposites towards Mcf-7 Cells. *RSC Adv.* **2015**, *5*, 1024–1032, https://doi.org/10.1039/C4RA11615A.
7. Akinyelu, J.; Singh,M. Folate-tagged chitosan functionalized gold nanoparticles for enhanced delivery of 5-fluorouracil to cancer cells. *Appl. Nanosci.* **2019**, *9*, 7-17, https://doi.org/10.1007/s13204-018-0896-4.
8. Geetanjali.; Sharma, P.K.; Malviya, R. Toxicity and application of nano-silver in multi-drug resistant therapy. *Lett. Appl. NanoBioSci.* **2020**, *9*, 824-829, https://doi.org/10.33263/LIANBS91.824829.
9. Khatami, M.; Sharifi,I.; Nobre, M.A.L.; Zafarnia, N.; Aflatoonian, M.R. Waste-grass-mediated green synthesis of silver nanoparticles and evaluation of their anti-cancer, antifungal and antibacterial activity. *Green Chem.Lett. Rev.* **2018**, *11*, 125-134, https://doi.org/10.1080/17518253.2018.1444797.
10. Milić, M.; Leitinger, G.; Pavicic, I.; Avdičević, M.Z.; Dobrović, S.; Goessler, W.; Vrček, I.V. Cellular uptake and toxicity effects of silver nanoparticles in mammalian kidney cells. *J.Appl.Toxicol.* **2015**, *35*, 581-592, https://doi.org/10.1002/jat.3081.
11. Mohammed, M.A.; Syeda, J.T.M.; Wasan, K.M.; Wasan, E.K. An Overview of Chitosan Nanoparticles and its Application in Non-Parenteral Drug Delivery. *Pharmaceutics* **2017**, *9*, https://doi.org/10.3390/pharmaceutics9040053.
12. Daniels A.N.; Singh, M. Sterically stabilised siRNA:gold nanocomplexes enhance c-MYC silencing in a breast cancer cell model. *Nanomedicine* **2019**, *14*, 1387–1401, https://doi.org/10.2217/nnm-2018-0462.
13. Ahmed, T.A.; Aljaeid, B.M. Preparation, Characterization, and Potential Application of Chitosan, Chitosan Derivatives, and Chitosan Metal Nanoparticles in Pharmaceutical Drug Delivery. *Drug Des. Devel. Ther.* **2016**, *10*, 483–507, https://doi.org/10.2147/dddt.s99651.
14. Hettiarachchi, M.A.; Wickramarachchi, P.A.S.R. Synthesis of chitosan stabilized silver nanoparticles using gamma ray irradiation and characterization. *J. Sci. Univ. Kelaniya* **2012**. *6*, https://doi.org/10.4038/josuk.v6i0.4222.
15. Muro, S. Challenges in Design and Characterization of Ligand Targeted Drug Delivery Systems. *J. Control. Release* **2012**, *164*, 125–137, https://doi.org/10.1016/j.jconrel.2012.05.052.
16. Huang, Y.W.; Cambre, M.; Lee, H.J. The Toxicity of Nanoparticles Depends on Multiple Molecular and Physicochemical Mechanisms. *Int. J. Mol. Sci.* **2017**, *18*, https://doi.org/10.3390/ijms18122702.
17. Turkevich, J.; Stevenson, P.C.; Hillier, J. A study of the nucleation and growth processes in the synthesis of colloidal gold. *Discuss. Faraday Soc.* **1951**, *11*, 55-75, https://doi.org/10.1039/DF9511100055.
18. Rashid, M.U.; Bhuiyan, M.K.H.; Quayum, M.E. Synthesis of Silver Nano Particles (ag-Nps) and Their Uses for Quantitative Analysis of Vitamin C Tablets. *Dhaka Univ. J. Pharm. Sci.* **2013**, *12*, 29–33, https://doi.org/10.3329/dujps.v12i1.16297.
19. Lazarus, G.G.; Revaprasadu, N.; López-Viota, J.; Singh, M. The electrokinetic characterization of gold nanoparticles, functionalized with cationic functional groups, and its interaction with DNA. *Colloids Surf. B Biointerfaces* **2014**, *121*, 425-431, https://doi.org/10.1016/j.colsurfb.2014.06.032.
20. Pathak, J.; Sonker, A.S.; Ragneesh; Singh,V.; Kumar, D.; Sinha, R.P. Synthesis of silver nanoparticles from extracts of *Scytonema geitleri* HKAR-12 and their *in vitro* antibacterial and antitumor potentials. *Lett. Appl. NanoBioSci.* **2019**, *8*, 576-585, https://doi.org/10.33263/LIANBS83.576585.
21. Seda Tığlı Aydın, R.; Pulat, M. 5-Fluorouracil Encapsulated Chitosan Nanoparticles for Ph-Stimulated Drug Delivery: Evaluation of Controlled Release Kinetics. *J. Nanomater.* **2012**, *2012*, https://doi.org/10.1155/2012/313961.
22. Craig, G.E.; Brown, S.D.; Lamprou, D.A.; Graham, D.; Wheate, N.J. Cisplatin-Tethered Gold Nanoparticles That Exhibit Enhanced Reproducibility, Drug Loading, and Stability: A Step Closer to Pharmaceutical Approval? *Inorg. Chem.* **2012**, *51*, 3490–3497, https://doi.org/10.1021/ic202197g.
23. Malloy, A. Count, Size and Visualize Nanoparticles. *Mater. Today* **2011**, *14*, 170-173, https://doi.org/10.1016/S1369-7021(11)70089-X.
24. Mosmann, T. Rapid colorimetric assay for cellular growth and survival: application toproliferation and cytotoxicity assays. *J. Immunol. Methods* **1983**, *65*, 55-63, https://doi.org/10.1016/0022-1759(83)90303-4.
25. Maiyo, F.; Singh, M. Polymerized Selenium nanoparticles for Folate-Receptor Targeted Delivery of anti-Luc-siRNA: Potential for Gene Silencing. *Biomedicines* **2020**, *8*, http://dx.doi.org/10.3390/biomedicines8040076.
26. Ribble, D.; Goldstein, N.B.; Norris, D.A.; Shellman, Y.G. A Simple Technique for Quantifying apoptosis in 96-Well Plates. *BMC Biotechnol.* **2005**, *5*, https://doi.org/10.1186/1472-6750-5-12.
27. Maiyo, F.; Moodley, R.; Singh, M. Cytotoxicity, antioxidant and apoptosis studies of Quercetin-3-O-glucoside and 4-(β-D-Glucopyranosyl-1→4-α-L-Rhamnopyranosyloxy)-benzyl isothiocyanate from *Moringa oleifera*. *Anti-cancer Agents Med.Chem.* **2016**, *16*, 648-656, http://doi.org/10.2174/1871520615666151002110424.
28. Queiroz, M.F.; Melo, K.R.T.; Sabry, D.A.; Sassaki, G.L.; Rocha, H.A.O. Does the Use of Chitosan Contribute to Oxalate Kidney Stone Formation? *Marine Drugs* **2014**, *13*, 141–158, https://doi.org/10.3390/md13010141.

29. Rizvi, S.A.A.; Saleh, A.M. Applications of nanoparticle systems in drug delivery technology. *Saudi Pharm. J.* **2018**, *26*, 64-70, https://doi.org/10.1016/j.jsps.2017.10.012.
30. Honary, S.; Zahir, F. Effect of Zeta Potential on the Properties of Nano-Drug Delivery Systems.-A Review (Part 2). *Trop. J. Pharm. Res.* **2013**, *12*, 265-273, https://doi.org/10.4314/tjpr.v12i2.20.
31. Jannathul, M.F.; Lalitha, P. Apoptotic Efficacy of Biogenic Silver Nanoparticles on Human Breast Cancer MCF-7 Cell Lines. *Prog. Biomater.* **2015**, *4*, 113-121, https://doi.org/10.1007/s40204-015-0042-2.
32. Huang, W.F.; Tsui, C.P.; Tang, C.Y.; Yang, M.; Gu, L. Surface Charge Switchable and Ph-Responsive Chitosan/polymer Core-Shell Composite Nanoparticles for Drug Delivery Application. *Compos. Part B* **2017**, *121*, 83-91, https://doi.org/10.1016/j.compositesb.2017.03.028.
33. Moodley, T,; Singh, M. Polymeric Mesoporous Silica Nanoparticles for enhanced delivery of 5-Fluorouracil in vitro. *Pharmaceutics* **2019** *11*, https://doi.org/10.3390/pharmaceutics11060288.
34. Moodley, T.; Singh, M. Sterically Stabilised Polymeric Mesoporous Silica Nanoparticles Improve Doxorubicin Efficiency: Tailored Cancer Therapy. *Molecules* **2020**, *25*, https://doi.org/10.3390/molecules25030742.
35. D'Arcy, M. Cell Death: A review of the major forms of Apoptosis, Necrosis and Autophagy. *Cell Biol. Int.* **2019**, *43*, 582-592, https://doi.org/1002/cbin.11137.
36. Van der Zande, M.; Undas, A.K.; Kramer, E.; Monopoli, M.P.; Peters, R.J.; Garry, D. Antunes Fernandes, E.C.; Hendriksen, P.J.; Marvin, H.J.P.; Peijnenburg, A.A.; Bouwmeester, H. Different Responses of Caco-2 and Mcf-7 Cells to Silver Nanoparticles Are Based on Highly Similar Mechanisms of Action. *Nanotoxicology* **2016**, *10*, 1431–144, https://doi.org/10.1080/17435390.2016.1225132.
37. Banerjee, K.; Rai, V.R.; Umarshankar, M. Effect of peptide-conjugated nanoparticles on cell lines. *Prog. Biomater.* **2019,** *8*, 11-21, https://doi.org/10.1007/s40204-019-0106-9.
38. Abdel-Fattah, W.I.; Ali, G.W. On the anti-cancer activities of silver nanoparticles.J Appl. Biotechnol. Bioeng. **2018**, *5*, 43-46, https://doi.org/10.15406/jabb.2018.05.00116.
39. Hepokur,C.; Kariper,I.A.; Misir,S.; Ay, E.; Tonoğlu, S.; Ersez, M.S.; Zeybek,U.; Kuruca, S.E.; Yaylim, I. Silver nanoparticle/capecitabine for breast cancer cell treatment. *Toxicol. in Vitro* **2019**, *61*, https://doi.org/10.1016/j.tiv.2019.104600.
40. He, Y.; Zhu, Q.; Chen, M.; Huang, Q.; Wang, W.; Li, Q.; Huang, Y.; Di, W. The Changing 50% Inhibitory Concentration (ic50) of Cisplatin: A Pilot Study on the Artifacts of the Mtt Assay and the Precise Measurement of Density-Dependent Chemoresistance in Ovarian Cancer. *Oncotarget* **2016**, *7*, 70803–70821, https://doi.org/10.18632/oncotarget.12223.
41. Szturz, P.; Cristina, V.; Gomez, R.G.H.; Bourhis, J.; Simon, C.; Vermorken, J.B.Cisplatin Eligibility Issues and Alternative Regimens in Locoregionally Advanced Head and Neck Cancer: Recommendations for Clinical Practice. *Front. Oncol*. **2019**, *9*, https://doi.org/10.3389/fonc.2019.00464.
42. George, B.P.A.; Kumar, N.; Abrahamse, H.; Ray, S.S. Apoptotic efficacy of multifaceted biosynthesized silver nanoparticles on human adenocarcinoma cells. *Sci. Rep*. **2018**, *8*, https://doi.org/10.1038/s41598-018-32480-5.
43. Nasr, R.; Hasanzadeh, H.; Khaleghian, A.; Moshtaghian, A.; Emadi, A.; Moshfegh, S. Induction of Apoptosis and Inhibition of Invasion in Gastric Cancer Cells by Titanium Dioxide Nanoparticles. *Oman Med. J.* **2018,** *33*, 111-117, https://doi.org/10.5001/omj.2018.22.